Liquefaction of humins from C6-sugar conversions using heterogeneous catalysts

Wang, Yuehu

2. Formation, Molecular Structure and Morphology of Humins in Biomass Conversion: Influence of Feedstock and Processing Conditions

ABSTRACT

Neither the routes through which humin byproducts are formed, nor their molecular structure have yet been unequivocally established. A better understanding of the formation and physicochemical properties of humins, however, would aid in making biomass conversion processes more efficient. Here, an extensive multiple-technique-based study of the formation, molecular structure, and morphology of humins is presented as a function of sugar feed, the presence of additives (e.g., 1,2,4-trihydroxybenzene), and the applied processing conditions. Elemental analyses indicate that humins are formed through a dehydration pathway, with humin formation and levulinic acid yields strongly depending on the processing parameters. The addition of implied intermediates to the feedstocks showed that furan and phenol compounds formed during the acid-catalysed dehydration of sugars are indeed included in the humin structure. IR spectra, sheared sum projections of solid-state 2DPASS ^{13}C NMR spectra, and pyrolysis GC–MS data indicate that humins consist of a furan-rich polymer network containing different oxygen functional groups. The structure is furthermore found to strongly depend on the type of feedstock. A model for the molecular structure of humins is proposed based on the data presented.

Keywords: Humins, synthesis, characterisation, structural models.

The results described in this Chapter were obtained in close collaboration with the Weckhuysen group of the University of Utrecht, The Netherlands. Yuehu Wang and Ilona van Zandvoort contributed equally to this chapter, it is therefore part of both PhD theses.

van Zandvoort Ilona, Wang Yuehu, Rasrendra Carolus B., van Eck Ernst R. H., Bruijnincx Pieter C. A., Heeres Hero J., Weckhuysen Bert M. Formation, molecular structure, and morphology of humins in biomass conversion: influence of feedstock and processing conditions. *ChemSusChem*. 2013. 6(9). 1745-1758.

2.1. INTRODUCTION

In a lignocellulosic biorefinery operation, the cellulose and hemicellulose fractions generally need to be depolymerised first to the individual glucose (C_6) and pentose units (C_5, for example, xylose) before the constituent monosaccharides can be further converted into a series of sustainable chemicals and fuels. A prominent example of such a subsequent conversion step is the acid-catalysed dehydration of glucose or xylose to form the key platform molecules 5-hydroxymethylfurfural (HMF) and furfural (FF), respectively.[1-5] Rehydration of HMF finally yields the valuable building blocks levulinic acid (LA) and formic acid (FA; Scheme 2-1).[3, 6] The strong current interest from industry in the production of HMF and LA-based chemicals is exemplified, for instance, by efforts of the Dutch company Avantium, which has recently announced the construction of a pilot plant to convert carbohydrates into various furanics. The so-called YXY furanics can subsequently be used as building blocks for the production of tailored polymers and biofuels.[7] The commercial-scale production of LA through the Biofine process is another well-known example.[8] Such acid-catalysed conversions of the (hemi-)cellulose fraction of lignocellulosic biomass to these platform chemicals are, however, unavoidably accompanied by the formation of so-called artificial humin byproducts, in short referred to as humins herein (Scheme 2-1).[9-11] Humins are carbonaceous, heterogeneous, polydisperse materials of which the molecular structure is largely unknown. For the Biofine process, it is known that humin formation decreases the yield of LA and poses considerable challenges in terms of reactor engineering.[8]

Humin byproducts have so far received very little attention with respect to the mechanism of the formation and elucidation of their molecular structure. Knowledge of both is nonetheless required if further optimization of the HMF or LA production processes, or, alternatively, the valorisation of the humins themselves is targeted. Indeed, herein, we aim to better understand the formation mechanism and to obtain insight into

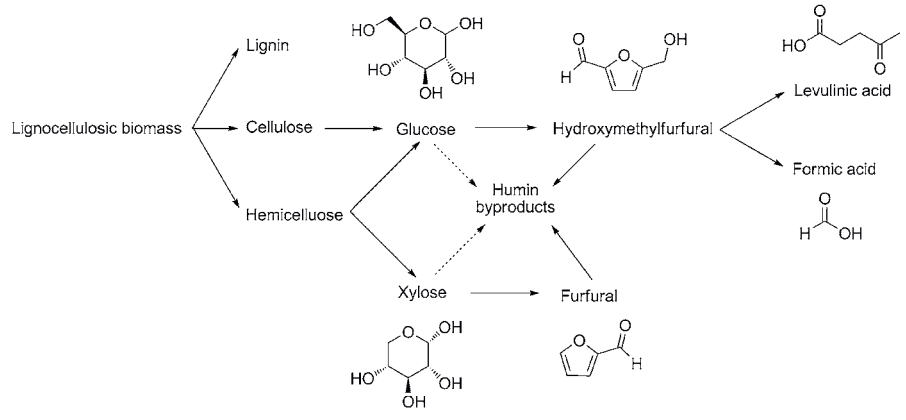

Scheme 2-1. Production of chemicals from lignocellulosic biomass and the related formation of humin byproducts by polymerisation of sugars and their derivatives.

the molecular structure and morphology of the humin byproduct. This information can then subsequently be used to limit the formation of, or to devise catalytic routes that valorise, the humins formed during biomass conversion processes.

To date, most knowledge about the structure of humin or humin-like components is based on the characterisation of functional carbon materials prepared by hydrothermal treatment of carbohydrates or biomass, so-called hydrothermal carbon (HTC).[12–14] This hydrothermal treatment differs from the above-mentioned processes that lead to humin formation because no acid is used in the formation of HTC. The structural insights obtained for HTC are nonetheless valuable because similar feedstock and conditions are involved. Two, somewhat conflicting, proposals for the molecular structure of HTC have been postulated. The molecular structures and relevant mechanisms proposed in the literature for HTC are reviewed below, and the processing conditions and HTC characterization data are summarised in Table 2-1.

Sevilla et al.[12, 13] studied the influence of reaction temperature, time, and feedstock on the structure of HTC. The amount of HTC formed during hydrothermal treatment increased with temperature, reaction time, and

(poly)saccharide concentration. The size and chemical composition of the spherical HTC particles depended strongly on the feed and processing parameters. XPS data showed that the O/C ratio of the surface of the particles was comparable to the bulk composition, as determined by elemental analysis, and indicated the presence of several reactive oxygen functional groups. With increasing temperature, the O/C and H/C ratio decreased; this suggested further carbonisation and aromatisation of the sample, which was supported by a decrease in the IR signals from oxygen functionalities at the expense of signals from aromatic rings. Also, the Raman spectra of the carbon material showed signals at 1360 and 1587 cm^{-1} that were attributed to the D and g bands of disordered graphite-like carbon. In addition, TEM images of HTC particles showed a slight difference in contrast between the core and the shell of the particle; this suggested a difference in chemical composition between the shell and core. A mechanism for the formation of HTC was proposed to involve condensation reactions between sugars and furanics formed during cellulose dehydration and subsequent aromatisation of the polymers. The resulting spherical particles were proposed to consist of a polyaromatic structure with hydrophilic groups on the surface and less reactive (hydrophobic) groups in the core.[12, 13] Shin and co-workers came to a similar conclusion regarding the structure after a study of the dehydration of fructose with Raman spectroscopy.[15] The spectroscopic data indicated the presence of aromatic groups with oxygen-rich functionalities. The presence of disordered carbon and graphite-like structures was confirmed by the D and g bands observed in the Raman spectra at 1385 and 1585 cm^{-1}, respectively. TEM images again showed spheres thought to consist of a condensed, hydrophobic core and a less dense, hydrophilic shell, in agreement with the structure suggested by Sevilla et al.[12, 13]

An alternative structure was suggested for various hexose- and pentose-derived HTC in a series of papers by the group of Titirici and Baccile.[14, 16, 17] Advanced solid-state (ss) ^{13}C NMR spectra of ^{13}C-labeled HTC led them to conclude that HTC consisted of a furan-rich structure in which subunits were directly bound to or linked together by an aliphatic group on the α

Table 2-1. Overview of the experimental conditions for HTC and humin production and techniques used for the characterisation of HTC and humin reported in the literature.

Ref.	Processing conditions					Characterisation
	Feedstock	[sugar]	[acid]	*T* (°C)	*t* (h)	Elemental composition
[13]	d-glucose sucrose starch	0.5-1 M 0.5 M 0.1-0.5 M	-	170-240 190 180-200	0.5-15	64.91 % C, 4.20 % H, 30.89 % O
[12]	cellulose	40-320 g/L	-	200-250	2-4	71.35 % C, 4.34 % H, 24.31 % O
[15]	d-fructose	2.5 M	-	120-140	0.5-2	-
[14]	d-glucose	10 wt%	-	180	24	62 % C, 4 % H, 34 %O
[16]	d-glucose HMF maltose sucrose amylopectin starch d-xylose FF	10 wt%	-	180	24	64.47 % C, 4.69 % H, 30.85 %O 68.58 % C, 4.11 % H, 27.31 % O
[26]	d-glucose cellulose rye straw	10 wt%	-	120-280	24	
[19]	d-xylose d-fructose sugar + phenolic compounds (1:1)	0.5 M total	-	130-170	12	61.2 % C, 4.1 % H, 34.7 % O
[23]	HMF	0.1-1.7 M	0-1 M H_2SO_4	98-181	≤10	61.2 % C, 4.5 % H
[27]	d-glucose HMF d-mannose d-galactose d- arabinose cellobiose methyl-α-d-glucoside	5 wt%	0.05 wt% H_2SO_4	175-180	2	66.4 % C, 4.7 %, H 28.9 % O
[28]	HMF	0.1 M	0-0.1 M H_2SO_4	118 125 135	0.25-2 18	-
[29]	HMF Glucose Fructose cellobiose	0.1 M	0.1 M H_2SO_4	118 125 135	0.5-24	-

Characterisation			
Particle Size	XPS Binding energy (eV)	IR Wavenumber (cm^{-1})	NMR δ (ppm)
0.4-6 µm	284.6 CH_x 285.7 C-OH C-O-C 287.2 C=O 289.0 COOH COOR 531.7 O=C 533.0 C-OH C-O-C	3000-3700 O-H 2900 C-H 1000-1450 C-O, 1620, 1513 875-750 C=C 1710 C=O	-
2–10 µm	284.6 CH_x 285.7 C-OH C-O-C 287.3 C=O 289.2 COOH COOR	3000-3700 O-H 2900 C-H 1000-1450 C-O 1620, 1513, 875-750 C=C 1710 C=O	-
200-400 nm	-	3500 OH 1704 COO^- 1604 C=C	Solid state: 100-230 aromatic functionality Liquid phase: fructose, formation of LA and HMF
-	-	-	Solid state: 13-74 sp^3 C 110-156 sp^2 C 175-179, 202-207, 218 C=O Liquid phase: HMF, LA, FA, glucose and dihydroxyacetone
500-1000 nm 100-1000 nm	-	-	208 C=O 175 C=O 150 C=C 40 aliphatic 20-40 methylene 75 C-OH 40-50 sp^3 C 129 C=C
glucose 160 °C 474 nm 260 °C 685 nm	-	1700 C=O Increases until 200-220 °C, disappears when T increases further	150 O-C=CH 110-118 O-C=CH 208 C=O 125-129 aromatic ring
	284.6 graphitic structures 286.0 C-OH C-O-C 288.4 C=O COOR 531.0 C=O 532.4 C-OH C-O-C	3400 O-H 1704 C=O 1616 C=C aromatic ring/furan 1290 1211 C-O-C 798 756 furan C-H out of plane def	-
5-10 µm	-	-	-
-	-	3500-3200 CH polymeric 2950-2800 CH aliphatic 1710-1685 furanic aromatic or aliphatic ester 1610-1650 furan 1440-1415 CH OH COO^- 1610-1360 furan ring 1200-1000 C-O-C	220-186 C=O 185-160 COOH 164-140 Furan-O 140-103 furan-H or –C 103-96 acetal 80-65 CH_2-O 58-54 CH_3-O
10 µm	-		-
	-	1710, 1625 C=O conjugated with C=C 1525, 1030, 850 and 750 furan ring	

or β position, with LA physically embedded in the polymer.[14] Data from carbonised sugars was compared to the characteristics of hydrothermally treated FF and HMF and showed that HTC produced from C_5 and C_6 sugars resembled carbonised FF and HMF, respectively. SEM images showed that different carbohydrates led to the formation of spheres with different particle sizes and elemental compositions. For example, HTC from xylose had a lower O/C and H/C ratio than that of HTC from the other starting materials.[16] The ^{13}C NMR spectra of xylose-based HTC also indicated a lower amount of aliphatic groups, and the signals attributed to conjugated C=C systems were stronger than those of glucose-derived HTC. This indicates that the molecular structure of HTC from C_5 sugars contains relatively more furanic moieties than HTC prepared from C_6 sugars.[16, 17]

1,2,4-Trihydroxybenzene (TB), a minor product formed from HMF during carbohydrate dehydration, has also been implicated in humin formation.[18] Suh *et al.* studied the effect of such phenolic compounds on the formation of HTC from sugars, demonstrating a substantial increase in carbon yield.[19] A twentyfold increase in carbon material formed was observed upon addition of 1,3,5-trihydroxybenzene, for instance. In addition, the spheres were larger than the particles prepared without aromatics in the feedstock. Addition of 1,3,5-trihydroxybenzene also increased the oxygen content of the HTC formed.

The formation and molecular structure of humin byproducts formed during acid-catalysed dehydration of sugars under conditions typical for biorefinery operations have been much less studied. Of the mechanistic studies on LA production by acid-catalysed dehydration of glucose and whole biomass, only a few research groups have developed kinetic models that include the formation of humins. Most prominent examples are the work of Kuster *et al.*[20–22] and Heeres *et al.*[9, 23–25] The Heeres group, for instance, included humin formation in a kinetic model for the production of LA from HMF and more complex feedstocks such as glucose, cellulose, and water hyacinth. The reaction conditions were optimised to obtain high LA yields, but the formation of humin byproducts could not be avoided.

The elemental composition of the humins formed during the production of LA from HMF was determined and SEM images were acquired; these showed that agglomerated, spherical particles with a diameter of 5–10 μm were formed.[23] However, further insight into the chemical structure of the humins was not obtained.

The molecular structure of humins formed during acid treatment of different carbohydrates and HMF was investigated by Sumerskii *et al.*[27] After isolation of the solids, the filtrate was neutralised to precipitate any acid-soluble polymers. About 20 wt % of the total amount of isolated humins could be dissolved in acetone, ^{13}C NMR and IR spectroscopic analysis of which showed it to have a similar chemical structure to the insoluble fraction and could, therefore, be regarded as shorter, less condensed polymeric precursors to insoluble humins. Based on the detection of several furan molecules by pyrolysis/GC–MS, it was concluded that the humins consisted of 60 % furan rings and 20 % aliphatic linkers. A mechanism for the formation of humin byproducts was proposed to involve a polycondensation pathway, leading to a network of furan rings linked by ether or acetal bonds.[27]

Lund et al.[28] reported the formation of humins and HTC from HMF. A kinetic model for the rehydration of HMF to LA, including the formation of humins, was proposed. The IR spectra of acid-catalysed and hydrothermal carbonization products indicated differences in the relative amount of functional groups. This, together with SEM images showing a different morphology of the HTC compared with the humins, indicates a difference in the formation mechanism. A mechanism for the formation of humins was proposed, involving 2,5-dioxo-6-hydroxyhexanal (DHH), formed by the rehydration of HMF, as a key intermediate. This intermediate was proposed to polymerise through subsequent aldol condensations with the carbonyl group of HMF to form humins (Scheme 2-2 A and B).[28] Recently, this work was continued by studying the differences between humins formed from HMF, glucose, fructose, and cellobiose. The particle size of the humins increased with reaction time. IR spectra, however, indicated that this was not related to a change in the molecular structure. It was found that humins

could not be directly formed from sugars. Instead, humins were proposed to be formed by aldol condensations between DHH and HMF, with the extent of incorporation of HMF in the humin structure being dependent on the accumulation of HMF during the acid-catalysed conversion of the sugars (Scheme 2-2 C).[29]

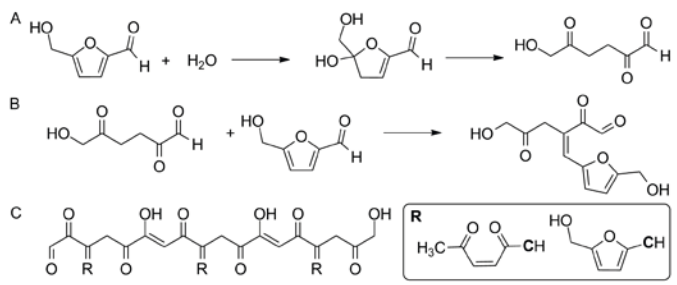

Scheme 2-2. A) Formation of DHH by the rehydration of HMF. B) Condensation of HMF with DHH. C) Idealised structure of humins formed through aldol condensation reactions of HMF with DHH, according to Lund *et al*.[28, 29]

A systematic study on the acid-catalysed formation of humins and the influence of both feed and process parameters on their molecular structure and morphology is not yet available. Indeed, most research is focused on either the conversion of C_6 sugars to LA and HMF or on the production of functional carbon materials from carbohydrates. Herein, we report on the conversion of (mixtures of) carbohydrates to the platform chemicals HMF, LA, or FF under various process conditions, as well as the extent of humin formation and their structural characteristics. The process conditions were chosen to fall within the operating window in which formation of humin byproducts is typically expected in a biorefinery operation. The Avantium process, for instance, treats a glucose-containing feedstock with 1-20 mol % of acid catalyst at 175-225 °C for 1–60 min.[30] In the Biofine process, on the other hand, lignocellulosic biomass is first hydrolyzed with 1.5-7 wt % H_2SO_4 at 210-250 °C for 7-30 s. Subsequently, HMF is rehydrated to form LA at 150-215 °C for 1-30 min.[8, 31, 32] In addition to a study of the influence of

these processing conditions and feedstock, the effect of addition of invoked intermediates, namely, HMF and TB, on the extent of formation and chemical structure of humins is reported.

The reaction products and humin samples were analysed by using several analytical techniques. The analytical tools utilised for the characterisation of humins are based on techniques for the analysis of HTC, soil samples, coal, and complex biomass samples. The bulk chemical composition of the humins was determined by elemental analysis. Chemical structure and functional group information was based on FTIR spectroscopy, pyrolysis/GC–MS, and ss NMR spectroscopy, whereas the morphology of the samples was analysed by SEM. This multiple parameter and multiple technique approach provides increased insight into the formation and chemical structure of humin byproducts as a function of feedstock and processing conditions and how this affects the production of furanics and LA from sugars.

2.2. RESULTS AND DISCUSSION

2.2.1. PREPARATION AND PURIFICATION OF HUMIN SAMPLES

Humin samples were prepared by acid-catalyzed dehydration of carbohydrates and purified according to the procedure depicted in Scheme 2-3. The solids were isolated by filtration and washed with a large excess of water to remove the remaining sugars, HMF, LA, and FA, and soluble humin precursors. This was not sufficient to remove all water-soluble compounds from the solid material; however, to allow for a fair comparison between the various humin samples, an extra purification step was necessary. A 24 h Soxhlet extraction with water (Scheme 2-3) did finally remove all water-soluble compounds from the humin samples.

Reaction conditions were chosen to fall within the window of a typical biorefinery operation. Longer reaction times were used, however, to obtain sufficient amounts of humin from the batch reactions for further

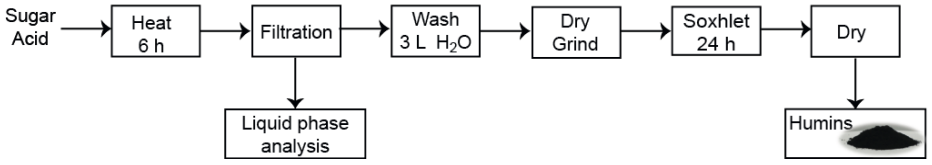

Scheme 2-3. Preparation and purification of humin samples.

characterisation. The influence of feedstock was studied through the preparation of humin samples from glucose, fructose, and xylose, along with mixtures of these carbohydrates under standard reaction conditions of 180 °C, a 1 M solution of sugar, and 0.01 M H_2SO_4. The influence of the proposed intermediates HMF and TB on humin formation was assessed through the addition of these compounds to the initial sugar feed (Table 2-2).

An additional study was performed for D-glucose to assess the effect of process conditions on the yields of humin obtained. This involved 17 experiments with temperature (113-247 °C), glucose concentration (0.66-2.34 M), and sulphuric acid concentration (0-0.13 M) as the independent variables at a fixed reaction time of 6 h (Table 2-3).

2.2.2. FORMATION OF HUMIN BY-PRODUCTS

The yield of humin byproducts was calculated as the number of grams of humin formed per 100 gram of feedstock (Table 2-2). The humin yield ranges from 30-39 wt % for the various sugars reacted under the standard conditions of 180 °C, 1 M sugar, and 0.01 M of acid. The acid-catalysed dehydration of fructose yielded more humins than glucose or xylose. The difference in humin yields between glucose and fructose can be attributed to the (on average) higher concentrations of HMF in solutions of fructose. That higher HMF concentrations lead to higher humin yields is in line with the route proposed by Lund and Patil, who reported humin formation to be first order in HMF.[28] A comparison of the humin yields of glucose

Table 2-2. Glucose conversion, yields, elemental composition of the humins, and the particle sizes formed during the acid-catalysed conversion of different feedstocks at 180 °C.

Sample	Feed	Conversion[a]	Yield[b]				Oligomers	Elemental composition		Particle size
		(mol %)	humins (wt%)	HMF (mol%)	FF (mol%)	LA (mol%)	M_w[c] (g/mol)	O/C	H/C	(µm)
Humin1	d-glucose	82	30	1	-	27	480	0.36	0.79	3-5
Humin2	d-fructose	100	39	< 1	-	31	400	0.36	0.76	5-7
Humin3	d-xylose	99	32	-	26	< 1	650	0.33	0.68	4-7
Humin4	d-glucose d-fructose 1:1[d]	95 100	36	< 1	-	31	270	0.35	0.77	4-7
Humin5	d-glucose d-fructose d-xylose 1:1:1[d]	98 99[e]	30	< 1	2	20	440	0.34	0.74	4-7
Humin6	d-glucose HMF 1:0.2[d]	95 98	30	< 1	-	29	420	0.34	0.76	4-7
Humin7	d-glucose TB 1:0.2[d]	88 100	39	< 1	-	17	380	0.39	0.70	3-5 1-2
Humin8	d-glucose TB 1:0.01[d]	98 100	34	< 1	-	23	460	0.39	0.78	6-8

[a] Conversion of sugars, HMF and TB in mol% [b] Humin yield determined as mass of humin formed from 100 g of starting material [c] Average molecular weight determined by GPC with maltose as a standard [d] Molar ratio [e] Conversion of both fructose and xylose: these carbohydrates cannot not separated by our HPLC protocol.

Table 2-3. Overview of glucose conversion and humin yields versus the process conditions used (6 h reaction time).

Run	*T* (°C)	[glucose] (m)	[acid] (m)	Conversion Glucose (mol%)	Humin Yield (wt%)
1	220	2.00	0.1	100	33
2	180	1.50	0.055	100	36
3	247	1.50	0.055	100	32
4	180	2.34	0.055	100	32
5	180	1.50	-	90	33
6	180	1.50	0.055	100	31
7	180	1.50	0.055	100	34
8	180	1.50	0.055	100	31
9	140	2.00	0.1	66	14
10	180	1.50	0.055	100	33
11	220	1.00	0.1	100	29
12	180	1.50	0.131	100	28
13	113	1.50	0.055	45	3
14	140	1.00	0.1	52	8
15	220	2.00	0.01	100	35
16	180	0.66	0.055	100	31
17	220	1.00	0.01	100	36

and xylose is less straightforward, but the results indicate that HMF is more reactive and prone to polymerisation than FF. The addition of HMF (1:0.2 glucose/HMF ratio, humin6) to the glucose feed did not affect the solid yield significantly. On the contrary, the addition of TB to the glucose feed (humin7 and humin8) clearly increased the extent of humin formation during acid-catalysed dehydration of glucose, as previously observed by Ryu *et al.*[19] The increase in humin formation indicates that TB functions as a cross-linker. It should be noted that the incorporation of TB in the humin cannot be accounted for with the mechanism proposed by Lund *et al.* for the formation of humins from HMF, in which aldol (condensation) reactions are proposed as the primary route for humin growth.[28]

To quantify the formation of humins from glucose as a function of processing parameters, a systematic study was performed, in which the range of conditions was selected by design of experiments (DoE; Table 2-3). The design contained five replicates (i.e., 180 °C, 1.50 M glucose, and 0.05 M H_2SO_4), and humin yields of these experiments were (33±2) wt %, indicative of a good reproducibility of the experiments. The results indicate that, in the chosen experimental window, humin formation mainly depends on temperature and to a lesser extent on the acid concentration. The glucose concentration is statistically not significant. Comparison with the literature shows that these conditions are opposite to those that lead to high LA yields.[24] The dependence of humin yield on temperature and acid concentration was statistically modeled and the result is depicted as a surface response plot in Figure 2-1. Agreement between experimental results and the model is satisfactory, as expressed by the R^2 value of 0.935.

The humin yield (in wt %) may be quantified by Equation 2-1:

$$humin\ yield = -120 + 1.507\,T - 63.58\ [H_2SO_4] - 3.56.10^{-3}\,T^2 \qquad (2\text{-}1)$$

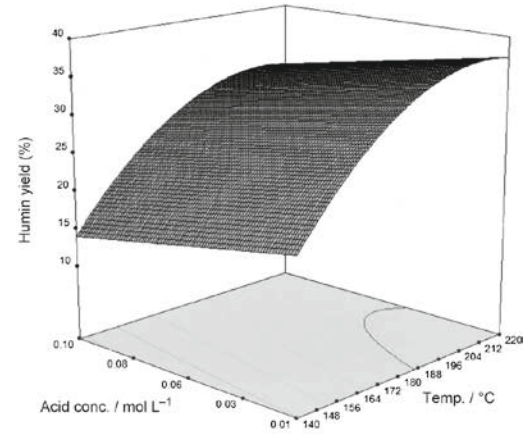

Figure 2-1. Surface response plot for the humin yield as a function of temperature and acid concentration (glucose concentration at 1.5 mol L^{-1}).

2.2.3. ELEMENTAL COMPOSITION OF HUMIN BY-PRODUCTS

The elemental compositions of humins prepared from different feedstocks are given in Table 2-2. The observed changes in atomic ratios during acid-catalysed dehydration of sugars are summarised in a van Krevelen diagram (Figure 2-2). The van Krevelen diagram allows one to determine what kinds of chemical transformations are taking place during product formation because elemental reactions, for example, dehydration, are represented by straight lines. The plot clearly shows that the elemental composition of the humin samples is the result of consecutive dehydration steps from the sugars via HMF. This implies that humins are formed by condensation reactions between sugars, HMF, and intermediates formed during the dehydration of carbohydrates. This plot also implies that the rehydration product, LA, is not incorporated in the humin structure to a large extent and that any occluded LA can be washed away by Soxhlet extraction.

The elemental composition of humin1 is slightly different from the elemental composition of glucose-derived HTC samples and humins found in the literature (Table 2-1). This can be attributed to differences in the

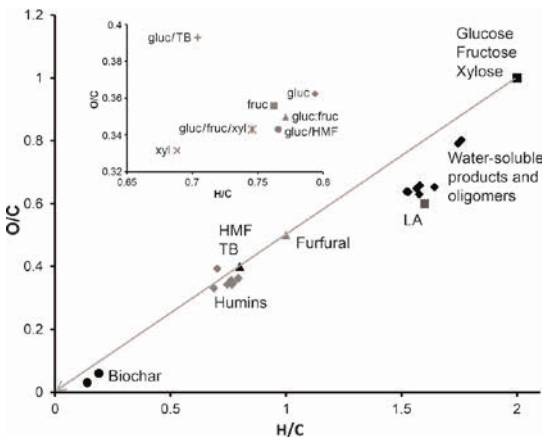

Figure 2-2. A van Krevelen plot depicting the changes in H/C and O/C ratio during acid-catalysed dehydration of sugars: carbohydrates (black squares), LA (grey squares), HMF and TB (grey triangles), FF (black triangles), water-soluble products and oligomers (black diamonds), humins (grey diamonds), and biochar (black dots). The elemental dehydration reaction is depicted by the grey arrow. The insert shows a magnification of the elemental composition of humins prepared from different feedstocks: gluc=glucose, fruc=fructose, and xyl=xylose.

processing parameters or washing procedure. Xylose-derived humin3 has lower H/C and O/C ratios than humins prepared from C_6 sugars; this indicates that fewer aliphatic linkers and fewer oxygen functional groups are present in the structure compared with the C_6-sugar-derived humins. The addition of HMF to the glucose feed barely changed the elemental composition of the humin. This, together with the spectroscopic evidence given below, is another indication that humins are mainly derived from HMF.

2.2.4. MORPHOLOGY OF HUMIN BY-PRODUCTS

Figure 2-3 shows, as an example, the scanning electron micrographs of samples of humin1, humin2, humin3, and humin7, which were prepared under the standard processing conditions, but with varying feedstocks; the particles sizes are reported in Table 2-2. The humins formed from C_6 sugars appear as spherical, interconnected particles of 3–5 μm in size. Humin2,

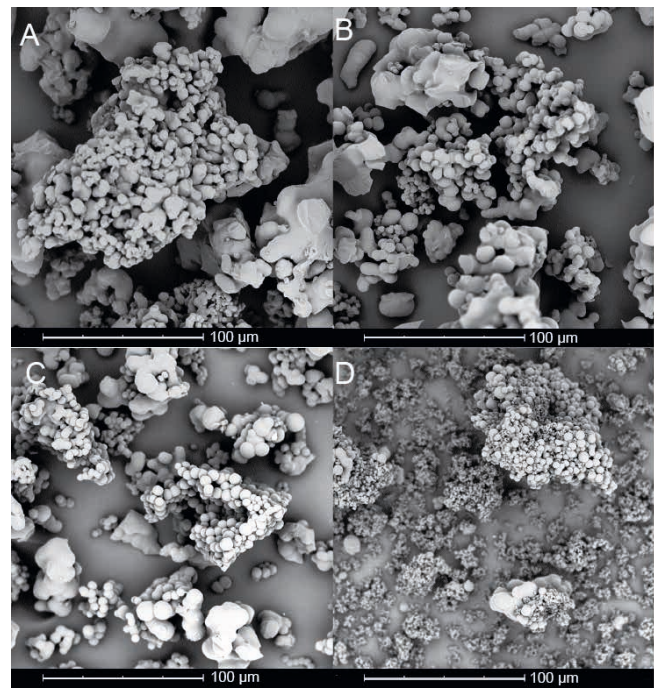

Figure 2-3. SEM micrographs of humins prepared from different feedstocks: glucose (A), fructose (B), xylose (C), and glucose/TB 1:0.2 (D).

formed from fructose, consists of slightly bigger particles than humin1, which is formed from glucose. The samples show some flattened particles and big lumps, which are believed to be formed as a result of collisions with the reactor wall and stirrer. Humin3 consists of spherical, isolated particles formed from xylose. Mixtures of carbohydrates lead to the agglomeration of particles, as clearly seen in the morphology of humin5 (Figure S1 in the Supporting Information). Compared with humin1, the addition of HMF to the reaction mixture leads to further agglomeration of the particles. The addition of 1 mol % TB (humin8) to the feedstock slightly increased the particle size of the humin (Figure S1 in the Supporting Information). On the other hand, the addition of 20 mol % TB (humin7) to the feedstock resulted in the formation of isolated, spherical particles. In this case, the majority of the particles were two or three times smaller than the particles formed

from pure glucose (Figure 2-3). This indicates that TB affects the crystallization/precipitation behavior of the humins, for instance, by changing the rates of nucleation and agglomeration.

These results show that the morphology of humin byproducts strongly depends on the composition of the feedstock. Comparable results, that is, the formation of interconnected and isolated particles from C_6 and C_5 sugars, respectively, were found for HTC.[16] However, the reported HTC particle sizes were much smaller than the humin particles formed during acid-catalysed dehydration (Tables 2-1 and 2-2). It should be noted that the protocols for the production of HTC are optimised to obtain small and monodisperse particles. Interestingly, phenolic additives were reported to have the opposite effect on HTC particle size because the HTC particle size increased upon the addition of phenol compounds.[19]

2.2.5. CHARACTERISATION OF LIQUID PHASE PRODUCTS

The liquid phase was sampled after the reaction and analysed by HPLC, GPC, NMR spectroscopy, and elemental analysis. The sugar conversions and yields of soluble dehydration products were determined by HPLC (Table 2-2). Carbohydrate conversion was lowest for glucose at 82%, whereas fructose and xylose showed almost full conversion of the carbohydrate. HMF yields were low for all C_6-sugar reactions, whereas LA yields were over 25%. The yield of FA was assumed to be equal to the yield of LA because LA and FA formed in a 1:1 ratio. As expected, the LA yield from fructose was higher because HMF could be formed directly from fructose without the isomerisation step required for glucose. The addition of TB to the feedstock led to a considerable decrease in the LA yield due to increased humin formation. The acid-catalysed dehydration of xylose yielded FF, in about 26% yield, rather than HMF. Although FF can, in principle, be converted into organic acids, these were not observed in the liquid phase. FF therefore accumulates in the liquid phase. Humin formation, however, barely increased

compared with dehydration of glucose; this indicates that FF is less reactive than HMF.

The sum of the humin yield and products detected by HPLC analysis did not complete the mass balance; this indicates the presence of water-soluble oligomers. Further analysis of the liquid phase was performed to detect the presence of any such water-soluble oligomers. For this purpose, the liquid-phase samples were dried and the recovered solids were redissolved in [D_6]DMSO for analysis by means of NMR spectroscopy. The ^{1}H and ^{13}C NMR spectra confirmed the presence of mainly LA. Elemental analysis of the dried aqueous phase showed slightly higher H/C and O/C ratios than those expected for pure LA (Figure 2-2), which indicated the presence of LA, FA, soluble oligomers, and residual sugar. Furthermore, it is an indication that initial dehydration reactions lead to water-soluble oligomers, which, upon further water loss, precipitate from solution to give an insoluble product. GPC analysis of the liquid phase confirmed the presence of such water-soluble oligomers and indicated that the relative average molecular weights of the water-soluble products and oligomers were between 300 and 500 g mol^{-1} for C_6-sugar-derived products (Table 2-2). This indicates that soluble humin precursors are relatively small oligomers, since, for example, HMF already has a molecular weight of 126.11 g mol^{-1}. In addition, it suggests that the solubility of the oligomers is already reduced considerably when the degree of oligomerisation is still relatively low, leading to water-insoluble products. The differences in average molecular weight indicate that the oligomer intermediates of humin formation differ in solubility, depending on the original sugar feed. The average molecular weight of xylose-derived products is higher, for instance, than those for glucose, indicating increased solubility. Fructose-derived liquid-phase products, on the other hand, have a lower average molecular weight than that of glucose-derived products, pointing at lower solubility of the fructose-derived oligomers in water, which is in agreement with higher humin yield and faster humin formation from fructose. The addition of TB to the feedstock also leads to faster humin formation, and thus, a lower average molecular weight of the water-soluble compounds.

2.2.6. MOLECULAR STRUCTURE: CHARACTERISATION BY IR AND NMR SPECTROSCOPY AND PYROLYSIS/GC-MS

The IR spectra of humins derived from several carbohydrates are shown in Figure 2-4. The spectra of glucose- and fructose-derived humins, humin1 and humin2, respectively, are very similar and several peaks could be assigned. A broad peak from C=O stretching of alcohols was observed at around 3400 cm^{-1}; weak contributions from an aliphatic C=H stretch were observed at around 2900 cm^{-1}; at 1700 cm^{-1} the C=O stretch from acids, aldehydes, and ketones was observed. Various contributions in the spectra could be ascribed to substituted furan rings, for example, at 1600 cm^{-1} a C=C stretch and at 1020 cm^{-1} a C=O stretch or furan ring deformation. The signals from C=H out-of-plane deformation at around 800 and 765 cm^{-1} could be ascribed to substituted furans. The IR spectra of the glucose-derived humins are very similar to the spectra of HTC and humins reported in the literature.[12, 13, 27-29, 33] The furan-rich structure is further supported by strong similarities with the IR spectrum of polyfurfuryl alcohol.[34-36] The IR spectra of humins reported by Lund *et al.* indicated differences between the IR spectra of humins derived from glucose and fructose at around 1500 and 1020 cm^{-1}, which they explained as differences in the amount of HMF included in the humin structure.[29] These differences were not observed between the spectra of humin1 and humin2. This can probably be explained by the difference in reaction conditions. The humins studied herein were produced at a higher reaction temperature, leading to faster glucose conversion and, on average, lower HMF concentrations during the reaction. Other experimental differences are related to the reaction times. Both humin1 and humin2 are formed during a reaction time of 6 h rather than waiting until a certain sugar conversion was obtained.

In the IR spectrum of xylose-derived humins, the furan C=C stretching vibration appears at 1595 cm^{-1} and is weaker than the one observed for C_6-sugar-derived humins. The peaks at around 791 and 751 cm^{-1}, assigned to the C-H out-of-plane deformation of furan, are relatively stronger and

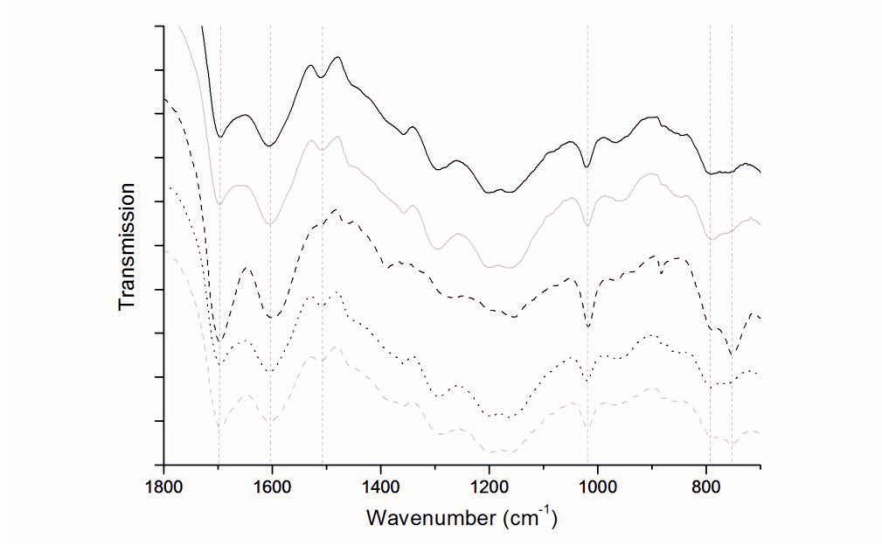

Figure 2-4. IR spectra of humins prepared from different carbohydrates and mixtures of carbohydrates: humin1 (black solid line), humin2 (grey solid line), humin3 (black dashed line), humin4 (black dotted line), and humin5 (grey dashed line).

sharper than those observed in the spectra of humin1 and humin2. This indicates a different substitution pattern of the furan rings. When fructose, glucose, and xylose are used as a mixed feedstock, both characteristic features from glucose- and xylose-derived humins can be observed in the IR spectrum of humin5. The addition of C_5 sugars to the feedstock thus leads to changes in the furan structure (Figure 2-4).

The addition of HMF to the feed barely led to any discernible changes in the IR spectrum of humin6, relative to glucose-derived humin1. This implies that the molecular structure of the two humins is very similar and that the humin structure, in turn, is mainly derived from HMF. On the contrary, the addition of TB led to significant differences in the IR spectrum (humin7). Compared with humin1, the broad signal in the C-O stretching region is narrower and shows a clear peak at 1200 cm^{-1}, which indicates the presence of phenolic OH groups. The signals from C-H out-of-plane deformation show an increase at around 856 cm^{-1} and a sharper peak at 798 cm^{-1}. These changes are ascribed to the contribution of C-H out-of-plane deformations

of 1,2,4-trisubstituted aromatic rings. It can, therefore, be concluded that TB is indeed included in the molecular structure, in which it probably functions as a cross-linker, and therefore, causes increased formation of humin byproducts (Figure 2-5).

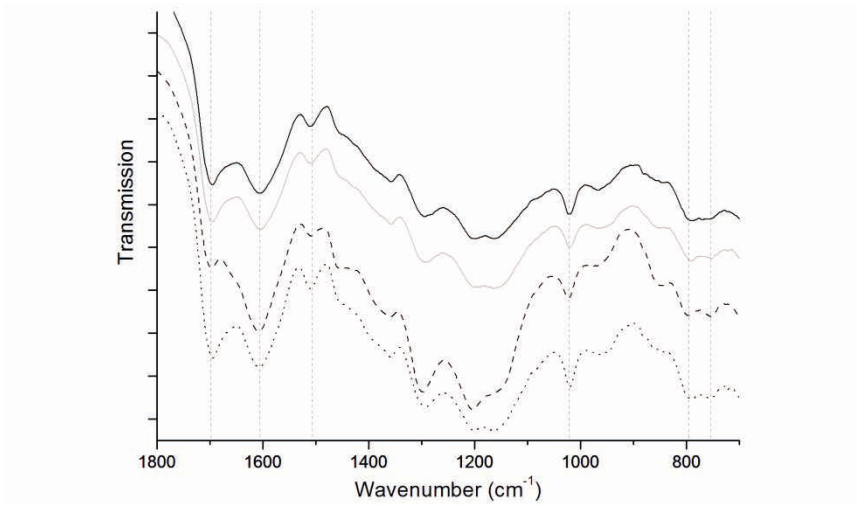

Figure 2-5. IR spectra of glucose humin and glucose humins with added intermediates: humin1 (black solid line), humin6 (grey solid line), humin7 (black dashed line), and humin8 (black dotted line).

The molecular structure of the humins was further studied by solid-state (ss) ^{13}C NMR spectroscopy. A common problem in ss NMR spectroscopy is that side bands arise from functional groups with a high anisotropy, such as carbonyl groups and aromatic rings. These side bands can overlap with main resonances and lead to erroneous interpretation. This can be addressed by using a high MAS speed, but this severely limits the amount of sample that can be used, and consequently, the signal-to-noise ratio suffers accordingly. Alternatively, a large sample volume can be used when spinning side bands are suppressed by using a total suppression of spinning side bands (TOSS) sequence,[37-40] but this method has the drawback that the signal intensity is lost from the anisotropic carbon atoms. To circumvent

this, a two-dimensional phase-adjusted spinning sidebands (2D PASS) sequence[41, 42] was employed herein, in which the spinning side bands were separated in a second dimension (Figure S2 in the Supporting Information). The cross polarisation-magic angle spinning (CP-MAS) NMR spectrum can then be reconstructed by summing the projections of the 2D spectrum. After shearing of the data, a side-band-free spectrum is obtained at low MAS speeds. This way, a side-band-free spectrum with high resolution can be obtained. This technique was particularly useful for the humin samples because several spinning side bands were located in important regions of the spectrum. The projections of the side bands only give an insight into their position and in the presence of anisotropic groups such as ketones and aromatic rings. The sheared sum projections of the 2D PASS NMR spectra of humins1-7 are shown in Figure 2-6. The NMR spectra can be divided into several areas: δ = 0-60 ppm aliphatic C, δ = 60-90 ppm C-O from ethers and alcohols (both regions representing sp^3-hybridized carbon atoms), δ = 90-160 ppm aromatic C (sp^2), and δ = 160-220 ppm C=O from carbonyl groups (sp^2).

Integration of the different areas in the NMR spectra of glucose- and xylose-derived humins did not reveal significant differences in the relative amounts of the chemical species: for glucose-derived humins, about 17 % of the carbon intensity is from alkanes, 53 % is from aromatics, and 13 % is from carbonyl groups. It is well known that the cross polarisation used to obtain the spectra results in the amount of non-protonated carbon atoms and methyl groups being underestimated.[43, 44]

Peak assignments for the humins are listed in Table 2-4. The region from δ = 0-60 ppm shows that saturated aliphatic groups are present in the structure of all humins. The spectra show a limited presence of methyl groups (15 ppm) and CH_2 linkers (around 30 ppm). This is in agreement with the IR spectra, which show a low intensity for C-H stretching from CH_2 and CH_3 groups. In comparison, the higher signal intensity observed between δ = 30 and 60 ppm is evident for a stronger presence of tertiary or quaternary aliphatic carbon atoms. Some intensity is also observed between δ = 70 and 90 ppm, which is a region typical for signals from alcohols and ethers.

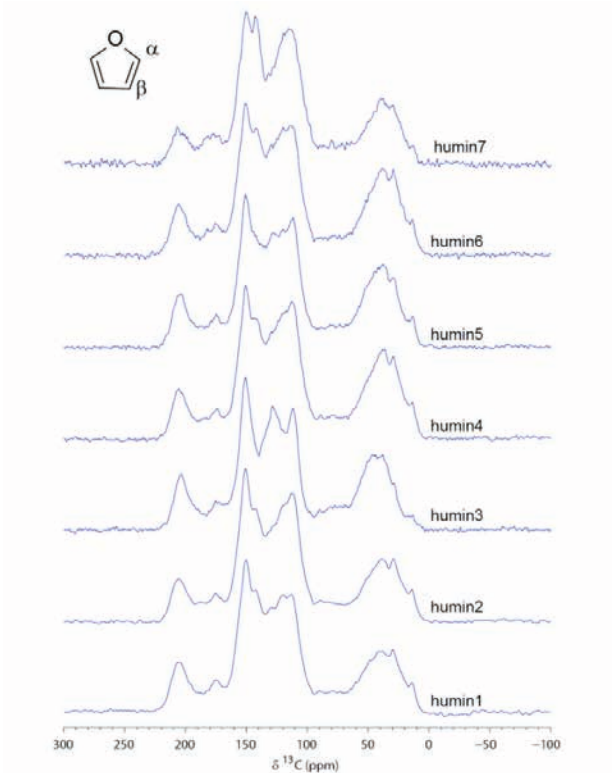

Figure 2-6. Sheared sum projections of the 2D PASS ^{13}C NMR spectra of humins prepared from different feedstocks. The α and β positions of furan are also highlighted.

The intensity in this region is broad, as a result of multiple, small contributions rather than large contributions from carbohydrates or HMF.[45] The aromatic region of the spectrum clearly shows that the humins do not consist of a graphite-like structure because an intense signal at around δ = 130 ppm would then be observed.[34] The signals at δ = 112, 120, and 128 ppm are ascribed to the β carbon of furan, linked β-carbon atoms, and conjugated structures, respectively. At δ = 142 ppm, signals from terminal furan α-carbon atoms are detected and linked α-carbon atoms are detected at δ = 150 ppm (Figure 2-6).[14, 34] Weak, yet distinct, signals are seen in the region between δ = 165 and 185 ppm. These signals could be from esters and acids as a result of ester formation or aldol condensations of LA or by acid formation due to

the ring opening of the furan units. A comparison with the IR spectra indicates that the amount of ester groups must be very low, although this makes an assignment to acid groups more likely. Finally, aldehydes and ketones are observed between δ = 195 and 220 ppm, which can, for instance, result from the aldehyde function in HMF, ketones formed as an intermediate in the rehydration of HMF (e.g., furan ring opening), or aldol condensation with ring-opening products such as DHH. The 2D PASS spectrum of glucose-derived humins is quite similar to the CP-MAS NMR spectrum of unlabeled HTC, as reported by Baccile *et al.*[14] The HTC sample does contain unreacted glucose, however, as indicated by a signal at around δ = 75 ppm, which is barely present in our humin samples. Further differences can be found in the region ascribed the signal from free CH_2 groups, which seem to be relatively more intense in the spectrum of HTC. In the aromatic region, the intensity at around δ = 130 ppm is slightly higher for humin1, which indicates a higher degree of conjugation in the humin sample.[14]

Table 2-4. Assignment of the signals in the ^{13}C NMR spectra of humins.

δ ppm	Functional group	Chemical formula
205	Ketone, aldehyde	C=O, HC=O
175	Acid, ester	COOH, COOR
150	α carbon furan linked	C=C-O
142	α carbon furan terminal	C=C-O
128	Furan conjugated	C-C=C-C
120	β carbon furan linked	C-C=C-O
112	β carbon furan	C-C=C-O
78	Alcohol, ether	C-OH, C-O-C
48	Aliphatic	C-H, C
39	Aliphatic	C-H, C
28	Aliphatic	$-CH_2-$
15	Aliphatic	$-CH_3$

The NMR spectra of glucose- and fructose-derived humins show that the humin structures must be similar. The relative signal intensities in

the aromatic region nevertheless differ, indicating differences in the substitution pattern of the furanic network. This is even more clearly seen in the NMR spectrum of the xylose-derived humin. Differences are indeed expected between the C_6 and C_5 sugars because the latter allow direct linking of the furan rings through the free 5-position of the FF intermediate. This results in a more extended conjugated network, which is indeed indicated by an increase in the intensity of the signal at around $\delta = 130$ ppm. An increase in signal intensity at around $\delta = 130$ ppm is also found when mixtures of C_6 sugars and xylose are used as feedstocks. A comparison with the literature shows that the same structures can be found in HTC derived from xylose.[16] The addition of HMF to the glucose feedstock led only to very minor changes in the NMR spectrum, again confirming that the humin formation pathway predominantly goes through HMF. The addition of TB leads to changes in the signals from arene/phenolic groups. It should be noted that signals from substituted furan α-carbon atoms and substituted carbon atoms in a phenolic ring, or furan β-carbon atoms and unsubstituted carbon atoms in a phenolic ring, are difficult to distinguish. Indeed, this is clearly illustrated by a comparison of the NMR spectrum of humin7 with the CP MAS NMR spectrum of a furanic-aromatic polyester.[46]

Finally, pyrolysis/GC–MS was performed on representative humin samples. A typical example of a chromatogram for a glucose-derived humin is given in Figure 2-7. It shows the presence of various furanics (e.g. 2-methylfuran, 2,5-dimethylfuran, FF), which is a strong indication of the presence of several furanic groups in the humin samples. Comparable products were observed during the pyrolysis of furfuryl alcohol resins; this further supports the furanic nature of humins.[47]

Based on the data presented above and by taking into account the structures previously reported for HTC, a polyfuranic molecular structure is proposed for C_6-sugar-derived humins (Figure 2-8 A). Given the highly heterogeneous nature of the humin's molecular structure, the structure drawn is intended to depict a representative fragment that includes the most important linkages. The proposed structure includes some features

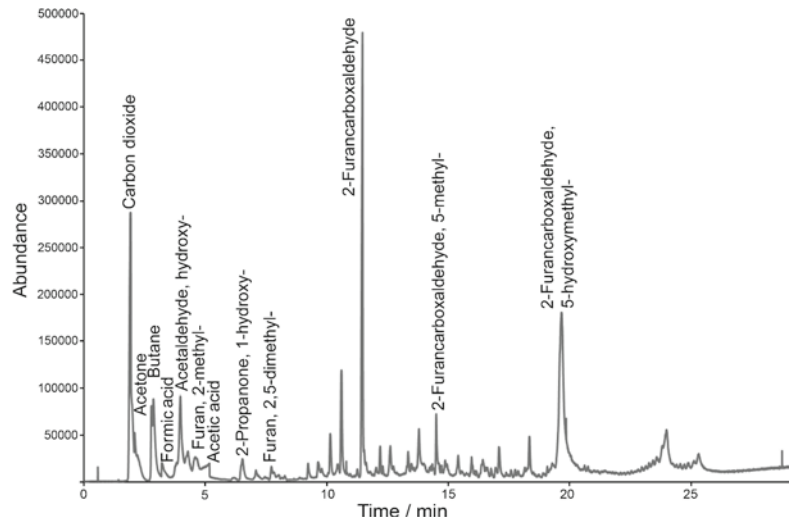

Figure 2-7. Pyrolysis/GC–MS chromatogram (600 °C) of a glucose-derived humin.

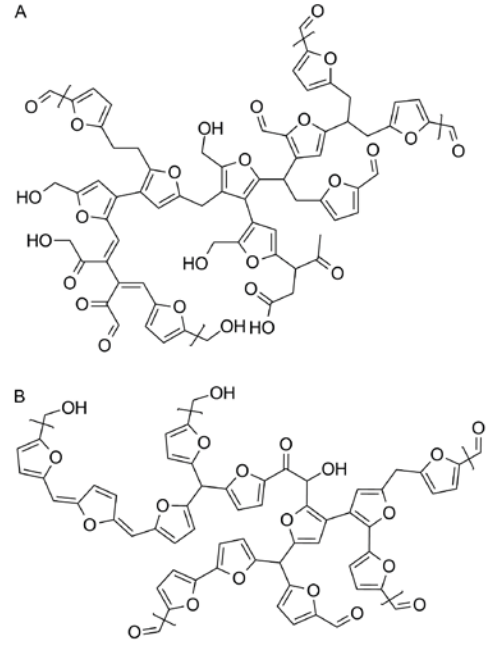

Figure 2-8. Model representing the molecular structure of a humin fragment, including the most important linkages for A) a glucose-derived humin and B) a xylose-derived humin.

of previously proposed HTC or humin structures, but also differs from them in important ways.[14, 28, 29] Substitution at the β position is thought to result from nucleophilic attack of the furan ring on the carbonyl group of HMF. Linking through the α position ocurs by condensation reactions between HMF molecules. The inclusion of rehydration products, such as DHH and, to a very limited extent, LA, ocurs through aldol condensations with the aldehyde functions of HMF or DHH itself.

The IR and NMR spectra also show that xylose-derived humins differ in molecular structure from glucose-derived humins. The free 5-position of FF allows for self-condensation reactions to ocur, leading to a structure in which furan units are linked by aliphatic CH_2 and CH groups, which is an option that is not available for humins formed from HMF as an intermediate. Further dehydration of this structure will lead to a polymer with more highly conjugated moieties, as indicated by our NMR spectra. As a result, the structure of a xylose-derived humin is expected to be more similar to the structure of FF resins, for which a structure was proposed by Gandini and Belgacem;[48] a model for xylose-derived humins structure is proposed in Figure 2-8 B. Linkage through the β position of FF is possible, however, less likely compared with HMF because the free 5-position of FF is more reactive than its β position.

The NMR spectra of our humins (derived from an acid-catalysed process) are very similar to those of HTC (derived from a non-acid-catalysed process), for which a structure was proposed by Baccile *et al.* with furanic units linked by CH_2 groups.[14] However, the elemental composition of this HTC model is in conflict with the van Krevelen plot (Figure 2-2), because the formation of this structure requires the loss of C atoms, involving a reaction other than dehydration. Our IR and NMR data furthermore show that the signals from CH_2 groups are weak. Also, the spectroscopic data provides no evidence for the significant presence of acetal bonds, which were suggested by Sumerskii *et al.*[27] as the linkages between the furanic rings. Elemental analyses also indicate that our humin samples are more dehydrated than Sumerskii's model suggests.[27] According to the model proposed by

Lund *et al.*,[28, 29] humins are formed through aldol condensations between HMF and DHH, with high HMF concentrations leading to a furan-rich humin. Our NMR spectroscopy data do not fully support this model, which does not contain any tertiary or quaternary carbon atoms. Furthermore, this model does not consider the presence of linked β carbon atoms, leading to the more cross-linked structures identified in our NMR spectroscopy data. Lund *et al.*[28, 29] also suggest that reactions with LA did not ocur. However, aldol condensation of HMF with the ketone group of LA is a plausible way to include a small amount of acids in the humin structure. Indeed, extracts of humin1 did not contain any LA, demonstrating that the observed signals from acid groups were not caused by physically embedded LA. Finally, the possibility of including TB in the humin structure also indicates that humins are not formed purely by aldol condensation reactions.[28, 29] The models presented in Figure 2-8 fit with the elemental composition as well as the spectroscopic characteristics of glucose- and xylose-derived humins.

2.3. CONCLUSIONS

The formation, morphology, and molecular structure of humin byproducts were studied as a function of feedstock and processing parameters. For the pure sugars, the acid-catalysed dehydration of fructose yielded the highest amount of humins because HMF was directly formed from fructose. Humin yields from xylose were slightly higher than those from glucose. During this reaction, FF accumulated in solution, indicating a lower propensity of FF to form organic acids and humin than that of HMF. The addition of TB to the feed led to an increase in humin formation, indicating that this molecule was included in the humin structure as a cross-linker. Furthermore, it showed that humin formation also involved reactions other than aldol condensations. The influence of acid concentration, sugar intake, and temperature on the formation of humins from glucose was studied by using a DoE-based approach. Data showed that humin formation was strongly influenced by

reaction temperature and acid concentration, but statistically barely depended on sugar concentration. Conditions for high humin production were opposite to those that would lead to high yields in LA. Analysis of the liquid phase by HPLC showed that LA was the main product formed from C_6 sugars, whereas C_5 sugars yielded FF. Furthermore, GPC analysis showed that water-soluble humin precursors were present in the liquid phase.

Humin samples prepared from different feedstock were characterised by several analytical techniques. SEM indicated that the humin byproducts had a spherical morphology, which strongly depended on feedstock and processing conditions. A study on the molecular structure of humin byproducts, through elemental analysis, IR spectroscopy, ss ^{13}C NMR spectroscopy, and pyrolysis/GC–MS, revealed a furanic structure with alcohol, acid, ketone, and aldehyde functional groups revealed a furanic structure, formed by a dehydration pathway, with alcohol, acid, ketone, and aldehyde functional groups. Based on this information, a model for the molecular structure for glucose-derived humins was proposed. Xylose-derived humins were found to have a more conjugated molecular structure. This could be explained by the free 5-position of FF, which led to the direct linking of furans, leading to fewer aliphatic groups and a more condensed network of furanic moieties.

The models for the molecular structure of the humins derived from C_5 and C_6 sugars presented herein will aid the development of catalytic routes for the valorisation of these byproducts. Indeed, humins can be seen as another recalcitrant feedstock that needs to be valorised to realise low-waste, competitive biorefinery processes. In this sense, analogy can be made with the development of valorisation strategies for lignin, which is another example of a recalcitrant, highly heterogeneous, aromatic biopolymer of limited solubility. Considerable advances in the structural characterisation of lignin, in particular, the type and ocurrence of specific linkages and the influence of pretreatment on the lignin structure, have clearly guided the development of catalytic lignin conversion strategies.[51] Similar advances are to be expected for the valorisation of humins. Pyrolysis, which is a process that

has been extensively studied for lignin, of humins is a promising example of this.[52] Alternatively, the insights gained in humin formation and structure can aid in managing the extent of humin formation, or can improve our understanding and application of related materials, such as biochars.

2.4. EXPERIMENTAL SECTION

Master batches of humin1–8 were prepared by heating an aqueous solution containing 1 M of carbohydrate (500 mL; D-glucose, D-fructose, D-xylose) and 0.01 M H_2SO_4 to 180 °C in a glass-lined 1 L batch reactor (Parr) for 6 h. The reactor was flushed with N_2 before heating. Humins were isolated by filtration, washed with water (3 L), dried under vacuum (0.3 mbar) for 12 h at 80 °C, and ground. After Soxhlet extraction with water for 24 h, the samples were dried for 24 h at 80 °C under vacuum. The yield of humin was calculated as the mass of solids formed per 100 g of starting material. For humin4 and humin5, prepared from mixtures of carbohydrates, that is, 1:1 glucose/fructose and 1:1:1 glucose/fructose/xylose, the total concentration was kept at 1 M. HMF and TB were added to the reaction mixture in a molar ratio of 1:0.2 sugar/aromatic with a total concentration of 1 m for humin6 and humin7. Humin8 was formed with TB added to the glucose feedstock in a 1:0.01 ratio.

The 17 humin samples for the DoE study were prepared in a 100 mL autoclave (Parr) by using glucose as the feed. Reaction conditions, that is, temperature (113-247 °C), glucose concentration (0.66-2.34 M), and H_2SO_4 concentration (0-0.13 M), were varied. A reaction time of 6 h was applied. The experimental humin yields were analyzed statistically by means of the Design Expert 8 software package (Stat-Ease Inc.). The response was modeled with a quadratic model by using the standard expression given by Equation 2-2:

$$y_k = b_0 + \sum_{i=1}^{3} b_i x_i + \sum_{i=1}^{3} b_{ii} x_i^2 + \sum_{\substack{i=1 \\ i \neq j}}^{3} \sum_{j=2}^{3} b_{ij} x_i x_j \qquad (2\text{-}2)$$

in which i represents the independent variables (temperature, acid concentration, and glucose concentration), whereas bi, bii, and bij are the regression coefficients obtained by statistical analyses of the data. The significant factors were selected based on their p value in the analysis of variance (ANOVA). Factors with a p value below 0.05 were regarded as significant and included in the response model. Stepwise elimination was applied to eliminate all statistically insignificant terms. After each elimination step, a new ANOVA table was generated until all insignificant factors were removed.

Humins and dried water-soluble products were analysed by using an automated Euro EA3000 CHNS analyzer. The oxygen content was calculated by difference. SEM images were recorded by using a Phenom G2 (FEI company) instrument. Samples were coated with 4 nm Pt with 10 % Pd. The liquid phase was analysed by using an Agilent HPLC system equipped with a Bio-Rad Aminex HPX-87H column, and a differential refractometer. The eluent was 5 mM H_2SO_4 and a flow rate of 0.55 mL min^{-1} was maintained at 60 °C with the detector temperature set to 40 °C. Further liquid-phase analysis was performed with an Agilent Technologies 1200 GPC system equipped with a ZORBAX Eclipse CDB-C18 Analytical (4.6×150 mm 5 µm) column. The system was operated at 23 °C with 5 mM $NaNO_3$ as a mobile phase and maltose was used as a standard. ^1H and ^{13}C NMR spectra were recorded in [D_6]DMSO with a Varian AS200 spectrometer.

ATR-IR spectra were recorded on a Bruker Tensor 37 IR spectrometer by using a diamond ATR crystal. For each spectrum, 32 scans with a resolution of 4 cm^{-1} were averaged. Two IR spectra were recorded for each humin sample and averaged.

The ss ^{13}C NMR spectra were recorded at the Radboud University of Nijmegen. All spectra were measured on a 300 MHz ss NMR spectrometer using a 7.5 mm double-resonant chemagnetics APEX probe, tuned at 75.45 MHz for carbon. All spectra were obtained by using ramped CPMAS at an rf-field of 55 kHz for carbon and 51 kHz for protons. Proton decoupling during acquisition was accomplished with a Spinal-64 sequence at an rf-field of 55 kHz, optimised to a pulse width and phase of 9 µs and 7°, respectively.

MAS speeds were 4 kHz, except for sample humin7, for which the speed was 3.2 kHz. After cross polarization, a 2D PASS sequence was used to separate the spinning side bands by employing cogwheel phase cycling.[50]

Analytical programmed temperature vaporization (PTV) GC–MS of humins was conducted with a HP 5890 GC Series II system equipped with a 5972 MS detector, and the PTV was controlled by an Optic 2 device. Typically 1 mg of sample was used. The pyrolysis temperature program was 40 °C for 2 min, then heating to 600 °C at a rate of 16 °C s^{-1}, and finally at 600 °C for 1 min. After pyrolysis, the products were transferred into a capillary column (Agilent Technologies VF-5ms, 30×0.25×1.0) by a GC injector (split 50:1). Helium was used as the carrier gas at a flow rate of 1 mL min^{-1}. The following GC temperature program was applied: starting temperature of 40 °C for 5 min followed by heating at a rate of 10 °C min^{-1} to a final temperature of 250 °C. The MS detector was operated in the electron ionisation mode (70 eV) with an interface temperature 280 °C. A scan range of m/z 35-400 was applied. Pyrolysis products were identified by comparison with mass spectra of authentic compounds and masses.

2.5. REFERENCES

1 van Putten RJ, van der Waal JC, de Jong E, Rasrendra CB, Heeres HJ, de Vries JG. Hydroxymethylfurfural, a Versatile Platform Chemical Made From Renewable Resources. *Chemical Reviews*. 2013; 113(3): 1499-1597.

2 Lange JP, van der Heide E, van Buijtenen J, Price R. Furfural-A Promising Platform for Lignocellulosic Biofuels. *ChemSusChem*. 2012; 5(1): 150-166.

3 Huber GW, Iborra S, Corma A. Synthesis of Transportation Fuels From Biomass: Chemistry, Catalysts, and Engineering. *Chemical Reviews*. 2006; 106(9): 4044-4098.

4 Corma A, Iborra S, Velty A. Chemical Routes for the Transformation of Biomass Into Chemicals. *Chemical Reviews*. 2007; 107(6): 2411-2502.

5 Wettstein SG, Alonso DM, Gürbüz EI, Dumesic JA. A Roadmap for Conversion of Lignocellulosic Biomass to Chemicals and Fuels. *Current Opinion in Chemical Engineering*. 2012; 1(3): 218-224.

6 Wettstein SG, Alonso DM, Chong Y, Dumesic JA. Production of Levulinic Acid and Gamma-Valerolactone (GVL) From Cellulose Using GVL as a Solvent in Biphasic Systems. *Energy & Environmental Science*. 2012; 5(8): 8199-8203.

7 Jong ED, Dam MA, Sipos L, Gruter GJM. Furandicarboxylic Acid (FDCA), a Versatile Building Block for a Very Interesting Class of Polyesters. American Chemical Society,2012,1-13.

8 Hayes DJ, Fitzpatrick S, Hayes MHB, Ross JRH. The Biofine Process–Production of Levulinic Acid, Furfural, and Formic Acid From Lignocellulosic Feedstocks.: *Wiley-VCH Verlag GmbH*, 2008, 139-164.

9 Girisuta B, Janssen LPBM, Heeres HJ. Kinetic Study On the Acid-Catalyzed Hydrolysis of Cellulose to Levulinic Acid. *Industrial & Engineering Chemistry Research*. 2007; 46(6): 1696-1708.

10 Horvat J, Klaić B, Metelko B, šunjić V. Mechanism of Levulinic Acid Formation. *Tetrahedron Letters*. 1985; 26(17): 2111-2114.

11 Lange JP, Price R, Ayoub PM, Louis J, Petrus L, Clarke L, Gosselink H. Valeric Biofuels: A Platform of Cellulosic Transportation Fuels. *Angew Chem Int Ed Engl*. 2010; 49(26): 4479-4483.

12 Sevilla M, Fuertes AB. The Production of Carbon Materials by Hydrothermal Carbonization of Cellulose. *Carbon*. 2009; 47(9): 2281-2289.

13 Sevilla M, Fuertes AB. Chemical and Structural Properties of Carbonaceous Products Obtained by Hydrothermal Carbonization of Saccharides. *Chemistry–A European Journal*. 2009; 15(16): 4195-4203.

14 Baccile N, Laurent G, Babonneau F, Fayon F, Titirici MM, Antonietti M. Structural Characterization of Hydrothermal Carbon Spheres by Advanced Solid-State MAS 13C NMR Investigations C-1835-2008. *Journal of Physical Chemistry C*. 2009; 113(22): 9644-9654.

15 Yao C, Shin Y, Wang L, Windisch CF, Samuels WD, Arey BW, Wang C, Risen WM, Exarhos GJ. Hydrothermal Dehydration of Aqueous Fructose Solutions in a Closed System. *The Journal of Physical Chemistry C*. 2007; 111(42): 15141-15145.

16 Titirici M, Antonietti M, Baccile N. Hydrothermal Carbon From Biomass: A Comparison of the Local Structure From Poly- to Monosaccharides and Pentoses/Hexoses. *Green Chemistry*. 2008; 10(11): 1204-1212.

17 Falco C, Caballero FP, Babonneau F, Gervais C, Laurent G, Titirici MM, Baccile N. Hydrothermal Carbon From Biomass: Structural Differences Between Hydrothermal and Pyrolyzed Carbons Via 13C Solid State NMR. *Langmuir*. 2011; 27(23): 14460-14471.

18 Luijkx GCA, van Rantwijk F, van Bekkum H. Hydrothermal Formation of 1,2,4-Benzenetriol From 5-Hydroxymethyl-2-Furaldehyde and D-Fructose. *Carbohydrate Research*. 1993; 242(0): 131-139.

19 Ryu J, Suh DJ, Suh Y, Ahn DJ. Hydrothermal Preparation of Carbon Microspheres From Mono-Saccharides and Phenolic Compounds. *Carbon*. 2010; 48(7): 1990-1998.

20 Kuster BFM. The Influence of Water Concentration On the Dehydration of D-Fructose. *Carbohydrate Research*. 1977; 54(2): 177-183.

21 Kuster B, Temmink H. Dehydration of D-Fructose (Formation of 5-Hydroxymethyl-2-Furaldehyde and Levulinic Acid).4. Influence of Ph and Weak-Acid Anions On Dehydration of D-Fructose. *Carbohydrate Research*. 1977; 54(2): 185-191.

22 Kuster B, Vanderbaan HS. Dehydration of D-Fructose (Formation of 5-Hydroxymethyl-2-Furaldehyde and Levulinic Acid).2. Influence of Initial and Catalyst Concentrations On Dehydration of D-Fructose. *Carbohydrate Research*. 1977; 54(2): 165-176.

23 Girisuta B, Janssen L, Heeres HJ. A Kinetic Study On the Decomposition of 5-Hydroxymethylfurfural Into Levulinic Acid. *Green Chemistry*. 2006; 8(8): 701-709.

24 Girisuta B, Janssen L, Heeres H. Green Chemicals: A Kinetic Study On the Conversion of Glucose to Levulinic Acid. *Chemical Engineering Research and Design*. 2006; 84(5): 339-349.

25 Girisuta B, Danon B, Manurung R, Janssen L, Heeres HJ. Experimental and Kinetic Modelling Studies On the Acid-Catalysed Hydrolysis of the Water Hyacinth Plant to Levulinic Acid. *Bioresource Technology*. 2008; 99(17): 8367-8375.

26 Falco C, Baccile N, Titirici MM. Morphological and Structural Differences Between Glucose, Cellulose and Lignocellulosic Biomass Derived Hydrothermal Carbons. *Green Chemistry*. 2011; 13(11): 3273-3281.

27 Sumerskii I, Krutov S, Zarubin M. Humin-Like Substances Formed Under the Conditions of Industrial Hydrolysis of Wood. *Russian Journal of Applied Chemistry*. 2010; 83(2): 320-327.

28 Patil S, Lund C. Formation and Growth of Humins Via Aldol Addition and Condensation During Acid-Catalyzed Conversion of 5-Hydroxymethylfurfural. *Energy & Fuels*. 2011; 25(10): 4745-4755.

29 Patil SKR, Heltzel J, Lund CRF. Comparison of Structural Features of Humins Formed Catalytically From Glucose, Fructose, and 5-Hydroxymethylfurfuraldehyde. *Energy & Fuels*. 2012; 26(8): 5281-5293.

30 Gruter GJM, Dautzenberg F.Method for the Synthesis of Organic Acid Esters of 5-Hydroxymethylfurfural and their Use. 2007-03-21; *Patent:* US20090131690 A1.

31 Fitzpatrick SW.Lignocellulose Degradation to Furfural and Levulinic Acid. 1988-04-26; *Patent:* US4897497A.

32 Fitzpatrick SW.Production of Levulinic Acid From Carbohydrate-Containing Materials. 1995-06-07; *Patent:* US5608105A.

33 Titirici MM, Thomas A, Yu S, Müller J, Antonietti M. A Direct Synthesis of Mesoporous Carbons with Bicontinuous Pore Morphology from Crude Plant Material by Hydrothermal Carbonization. *Chemistry of Materials*. 2007; 19(17): 4205-4212.

34 Burket CL, Rajagopalan R, Marencic AP, Dronvajjala K, Foley HC. Genesis of Porosity in Polyfurfuryl Alcohol Derived Nanoporous Carbon. *Carbon*. 2006; 44(14): 2957-2963.

35 Hernandez V, Ramirez FJ, Zotti G, López Navarrete JT. Resonance Raman and FTIR Spectra of Pristine and Doped Polyconjugated Polyfuran. *Chemical Physics Letters*. 1992; 191(5): 419-422.

36 En S, Bardak B, Yavuz AEG, g K AEU. Polyfuran/Zeolite LTA Composites and Adsorption Properties. *European Polymer Journal*. 2008; 44(8): 2708-2717.

37 Dixon WT. Spinning-Sideband-Free and Spinning-Sideband-Only Nmr-Spectra in Spinning Samples. *Journal of Chemical Physics*. 1982; 77(4): 1800-1809.

38 Dixon WT, Schaefer J, Sefcik MD, Stejskal EO, Mckay RA. Total Suppression of Sidebands in Cpmas C-13 Nmr. *Journal of Magnetic Resonance*. 1982; 49(2): 341-345.

39 Olejniczak ET, Vega S, Griffin RG. Multiple Pulse Nmr in Rotating Solids. *Journal of Chemical Physics*. 1984; 81(11): 4804-4817.

40 Song ZY, Antzutkin ON, Feng XL, Levitt MH. Side-Band Suppression in Magic-Angle-Spinning Nmr by a Sequence of 5 Pi Pulses. *Solid State Nuclear Magnetic Resonance*. 1993; 2(3): 143-146.

41 Antzutkin ON, Shekar SC, Levitt MH. 2-Dimensional Side-Band Separation in Magic-Angle-Spinning Nmr. *Journal of Magnetic Resonance*. 1995; 115(1): 7-19.

42 Vogt FG, Gibson JM, Aurentz DJ, Mueller KT, Benesi AJ. Multiple-Rotor-Cycle 2D PASS Experiments with Applications to 207Pb NMR Spectroscopy. *Journal of Magnetic Resonance*. 2000; 143(1): 153-160.

43 Frund R, Ludemann HD. The Quantitative Analysis of Solution-C-13 and Cp-mas-C-13 Nmr-Spectra of Humic Material. *Science of the Total Environment*. 1989; 81-2: 157-168.

44 Kinchesh P, Powlson DS, Randall EW. 13C Nmr-Studies of Organic-Matter in Whole Soils .1. Quantitation Possibilities. *European Journal of Soil Science*. 1995; 46(1): 125-137.

45 Pfeffer PE, Hicks KB, Frey MH, Opella SJ, Earl WL. Complete Solid-State 13C Nmr Chemical-Shift Assignments for Alpha-D-Glucose, Alpha-D-Glucose.H2O and Beta-D-Glucose. *Journal of Carbohydrate Chemistry*. 1984; 3(2): 197-217.

46 Gomes M, Gandini A, Silvestre AJD, Reis B. Synthesis and Characterization of Poly(2,5-Furan Dicarboxylate)s Based On a Variety of Diols. *Journal of Polymer Science Part A-Polymer Chemistry*. 2011; 49(17): 3759-3768.

47 Sanchez R, Hernandez C, Jalsovszky G, Czira G. Thermal-Degradation of Furfuraldehyde Resins-Pyrolysis-Gas Chromatography-Mass Spectrometry and Fourier-Transform Infrared. *European Polymer Journal*. 1994; 30(1): 37-42.

48 Gandini A. Furans in Polymer Chemistry. *Progress in Polymer Science*. 1997; 22(6): 1203-1379.

49 Terada I, Takeda T, Kobayashi T, Hiramoto T.Flavor Improving Agent and Food Or Drink Containing the Same. 2006-10-06; *Patent:* EP2070917B1.

50 Ivchenko N, Hughes CE, Levitt MH. Application of Cogwheel Phase Cycling to Sideband Manipulation Experiments in Solid-State NMR. *Journal of Magnetic Resonance*. 2003; 164(2): 286-293.

51 Zakzeski J, Bruijnincx PC, Jongerius AL, Weckhuysen BM. The Catalytic Valorization of Lignin for the Production of Renewable Chemicals. *Chemical Reviews*. 2010; 110(6): 3552-3599.

52 Rasrendra CB. Platform Chemicals From Biomass. *University of Groningen (NL)*. 2012; PhD thesis.

2.6. SUPPORTING INFORMATION

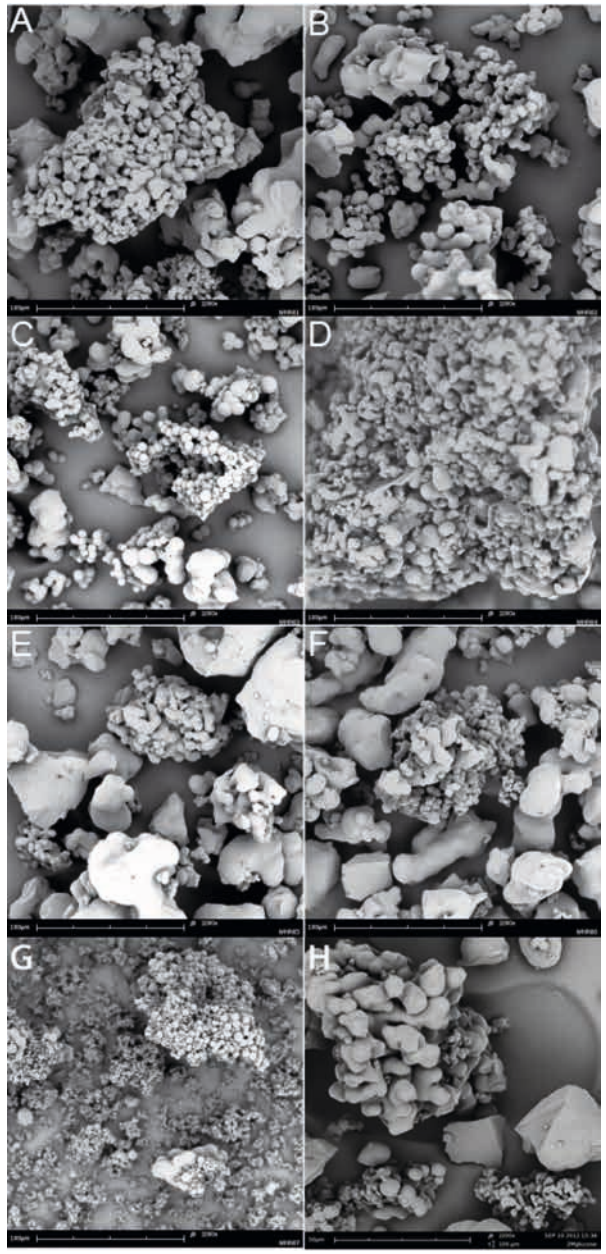

Figure S2-1. SEM images of humin1 (A), humin2 (B), humin3(C), humin4 (D), humin5 (E), humin6 (F), humin7 (G) and humin8 (H).

MORPHOLOGY OF HUMINS

Figure S2-1 shows the SEM of the samples humin1-8, which were prepared under the standard processing conditions, but with varying feedstock.

MOLECULAR STRUCTURE OF HUMINS

A ^{13}C CPMAS 2D PASS sequence was employed, in which the spinning sidebands are separated in a second dimension. Figure S2-2 shows the separation of the sidebands and centerbands from the 2D PASS NMR spectrum of a glucose-derived humin. By shifting the sidebands with the appropriate amount one can add the spectra to obtain the spinning sideband free spectra as in in Figure 2-6 of the manuscript.

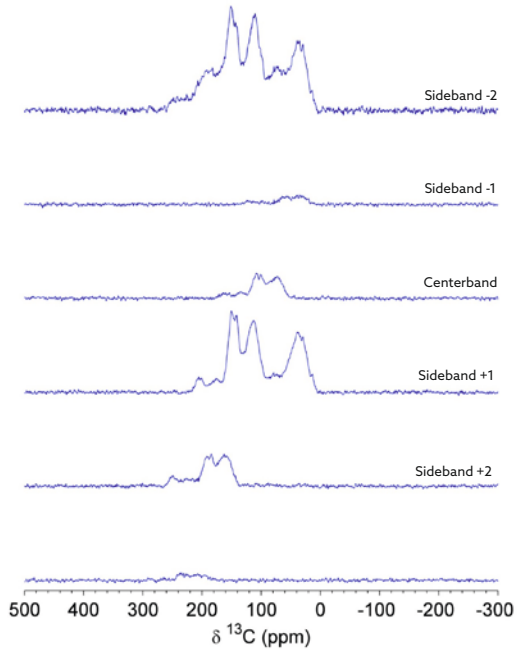

Figure S2-2. Projections of the spinning sidebands and centerbands, obtained by from 2D PASS NMR spectrum of glucose-derived humins.